Journal of Southeast University (English Edition) Vol. 41, No. 1, pp. 37-43 Mar. 2025 ISSN 1003-7985

Analysis of wind-induced vibration response characteristics of multispan double-layer cable photovoltaic support structure

ZOU Lianghao[1], WANG Jian[1], SONG Jie[1], ZHOU Rui[2], WANG Hao[2]

(1. School of Civil Engineering, Wuhan University, Wuhan 430072, China; 2. Key Laboratory of Concrete and Prestressed Concrete Structure of Ministry of Education, Southeast University, Nanjing 211189, China)

Abstract: To investigate the wind-induced vibration response characteristics of multispan double-layer cable photovoltaic (PV) support structures, wind tunnel tests using an aeroelastic model were carried out to obtain the wind-induced vibration response data of a three-span four-row double-layer cable PV support system. The wind-induced vibration characteristics with different PV module tilt angles, wind speeds, and wind direction angles were analyzed. The results showed that the double-layer cable large-span flexible PV support can effectively control the wind-induced vibration response and prevent the occurrence of flutter under strong wind conditions. The maximum value of the wind-induced vibration displacement of the flexible PV support system occurs in the windward first row. The upstream module has a significant shading effect on the downstream module, with a maximum effect of 23%. The most unfavorable wind direction angles of the structure are 0° and 180°. The change of the wind direction angle in the range of 0° to 30° has little effect on the wind vibration response. The change in the tilt angle of the PV modules has a greater impact on the wind vibration in the downwind direction and a smaller impact in the upwind direction. Special attention should be paid to the structural wind-resistant design of such systems in the upwind side span.

Key words: double-layer cable; photovoltaic support; aeroelastic model; wind tunnel test; wind-induced vibration response

DOI: 10.3969/j.issn.1003-7985.2025.01.005

Solar energy, as a renewable energy source, is favored for its wide distribution, nonpollution, and sustainable use. Photovoltaic (PV) power generation, as one of the important forms of solar energy utilization, has been widely applied and promoted worldwide. In recent years, due to the shortage of suitable land resources, PV power stations have been developing toward high clearance and large spans. Additionally, the increasing development of fishery-solar and agricultural-solar complementary PV projects in many regions has further driven this trend. Under these circumstances, developing large-span PV module support structures is necessary to meet these complex terrains.

As an emerging PV support system, the flexible PV support structure was first proposed by Baumgartner et al.[1] in 2008, introducing the Solar Wings method, which utilizes steel cables as the installation system for PV modules to enhance power generation efficiency. However, the cable system is also characterized by large flexibility and low damping and is thus prone to large vibrations under wind excitation[2-4]. Tamura et al.[5] and Kim et al.[6] conducted wind tunnel tests on the solar wing system, discovering the trend of fluctuating displacements under specific wind speeds and directions. Wang et al.[7-8] revealed that adding rigid rods between rows effectively reduces the displacement response of the structure. Liu[9] investigated two types of flexible PV support with elastic wind-resistant cables, exploring various parameters affecting wind vibration coefficients. Focusing on the wind load issues of flexible PV support structures, Chai[10] and Ma et al.[11] showed that the inclination angle of the components can significantly impact their wind loads, with the wind loads of the components in the middle of the PV array being significantly lower than those at the array edges. Wang[12] and Yang[13] studied the wind load distribution and interference effects on flexible PV support systems through numerical simulations. Chen et al.[14] examined the aerodynamic stability of flexible PV support through wind tunnel tests, finding poor flutter stability at 10° inclination and wind directions of 0°, 15°, and 30°. Xu et al.[15] revealed the sensitivity and variation rule of aerodynamic damping characteristics of large-span PV support structures under different conditions. Zhou et al.[16] investigated the effects of wind speed, wind direction, and cable pretension

Received 2024-07-03, **Revised** 2024-09-18.

Biographies: Zou Lianghao (1979—), male, doctor, associate professor; Wang Hao (corresponding author), male, doctor, professor, wanghao1980@seu.edu.cn.

Foundation item: The National Natural Science Foundation of China (No. 52338011).

Citation: ZOU Lianghao, WANG Jian, SONG Jie, et al. Analysis of wind-induced vibration response characteristics of multispan double-layer cable photovoltaic support structure[J]. Journal of Southeast University (English Edition), 2025, 41(1): 37-43. DOI: 10.3969/j.issn.1003-7985.2025.01.005.

on the wind resistance reliability of flexible PV support. Due to the significant wind-induced responses and poor flutter stability of single-layer cable-supported flexible PV structures in large spans, He et al. [17], Ding et al. [18], and Liu et al. [19] investigated the wind-induced vibration characteristics of a new double-layer cable-supported PV system through wind tunnel tests, discovering its stronger wind resistance and smaller settlement. Li et al. [20] proposed wind load reduction coefficients for different array regions and deeply analyzed the gust load factors. Additionally, Wang et al. [21] found that changes in the wind attack angle and cable prestress significantly affect the system's vibration characteristics. Fu et al. [22] demonstrated the aerodynamic characteristics and wind pressure distribution of double-row flexible PV support, filling in the blanks of the wind load calculation method.

However, previous studies on the interference effects of different rows, spans, wind direction angles, and wind attack angles on PV array systems have obtained different wind-induced response characteristics, and studies on multispan PV array systems have primarily focused on the wind-induced vibration response of a single span or a specific span. Therefore, a three-span, four-row, double-layer cable-supported flexible PV system will be used as the research object. A series of wind tunnel vibration tests will be conducted using an aeroelastic model under various module tilt angles, wind speeds, and wind direction angles. Vertical displacement time history data of PV modules in different spans will be obtained to further analyze their wind-induced vibration characteristics. This research will provide important insights and references for the wind-resistant design of such large-span flexible PV support structures.

1 Wind Tunnel Tests

1.1 Test model and instrument layout

The test model was designed and produced based on a three-span, four-row, double-layer cable-supported large-span flexible PV support structure. The span, height, and row spacing of the single-span prototype structure were 35, 4, and 2.5 m, respectively. Each row contained 28 PV modules, with individual module dimensions of 2 256 mm × 1 134 mm × 40 mm (length × width × thickness). The module tilt angles can be adjusted to 10°, 20°, and 30°. The PV modules were anchored to two main cables, which were connected to the lower stabilizing cable via triangular braces. The adjacent rows of the PV array were connected by horizontal linkers in three sections (i.e., 1/4 to 3/4 spans). The prototype structure is shown in Fig. 1. The design tension values for the main cables and stabilizing cables are 60 and 10 kN, respectively.

The model PV modules were made of balsa wood,

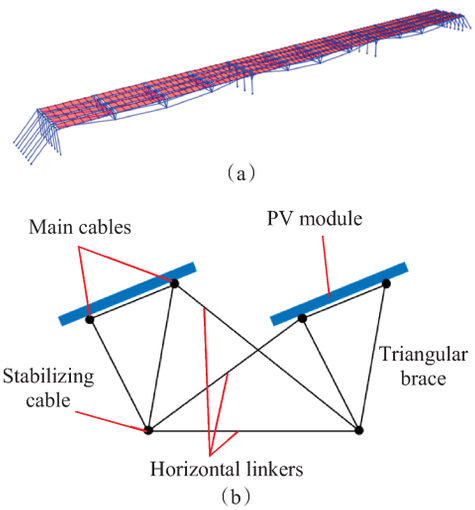

Fig. 1 Schematic diagram of the prototype structure. (a) Finite element model (FEM); (b) Cross-section details of adjacent rows

while the main and stabilizing cables were made of steel wires with an elastic modulus similar to that of the prototype. Both the triangular braces and the horizontal linkers were made of steel rods. The geometric scale ratio of the model was 1∶45, and the wind speed scale ratio was 1∶6.71, with the maximum blockage ratio in the test being less than 1%. Finite element calculations using SAP2000 determined the first vertical bending frequency of the prototype structure to be 1.25 Hz. Prior to the tests, pretension was applied to the cables using a spring dynamometer, which was calibrated to match the cable forces specified in the design model. The pretension was then fine-tuned by adjusting the vertical bending fundamental frequency of the test model to align with the design value obtained from the finite element model (FEM), ensuring that the frequency matched the intended design specification. Specific aeroelastic model parameters are listed in Table 1.

To measure the most adverse wind-induced responses of the PV aeroelastic model, laser displacement sensors were installed above the model. Targets were positioned at the geometric centers of the PV modules located in the middle of the side span and the middle span of each row. During the test, the laser of the displacement sensor was ensured to be vertically aligned with the pre-attached targets on the PV module surfaces to guarantee measurement accuracy. The sampling duration for the laser displacement sensors was 60 s, with a sampling frequency of 500 Hz per measurement point. The arrangement of the test model and displacement measurement points is shown in Fig. 2. The displacement measured by the laser displacement sensors represents the vertical displacement of the PV panels (i.e., downward is positive; upward is negative). The time history of vertical displacement free decay and the corresponding power spectral density are

Table 1 Parameters of the aeroelastic model

Item		Scale ratio	Prototype	Design model	Real model
Array system	Dimension/(m × m × m)	1∶45	35 × 8.85 × 4	0.78 × 0.20 × 0.09	0.78 × 0.20 × 0.09
PV module	Dimension/(m × m × m)	1∶45	2 256 × 1 134 × 40	50.13 × 25.20 × 0.89	50 × 25 × 2
	Mass/g	1∶91 125	44 651	0.49	0.50
Main cable	Tension/N	1∶91 125	60 000	0.66	0.66
Stabilizing cable	Tension/N	1∶91 125	10 000	0.11	0.11
First-order vertical bending frequency/Hz		6.71∶1	1.25	8.37	8.23

shown in Fig. 3. The damping ratio of the model was identified at 3.3%. The first vertical bending frequency from the free vibration test is 8.23 Hz, which is slightly lower than the FEM result with a calculated error of 1.7%.

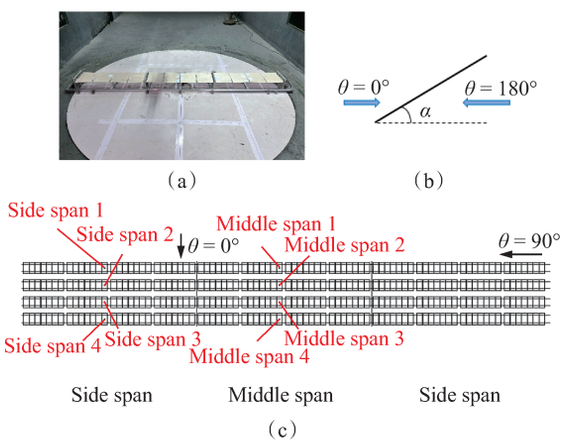

Fig. 2 Details of aeroelastic wind tunnel test. (a) Aeroelastic test model; (b) Module tilt angle and wind azimuth; (c) Layout of measurement points

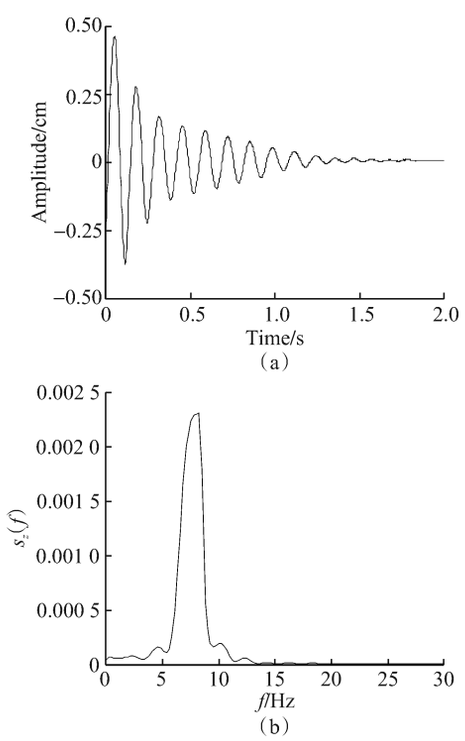

Fig. 3 Free vibration decay and power spectral density curves. (a) Free vibration decay; (b) Power spectral density

1.2 Test cases

All tests were conducted in the WD-1 Wind Tunnel Laboratory of Wuhan University, simulating the boundary layer wind field of Category B terrain, and the corresponding wind profile and wind spectrum are shown in Fig. 4. The turbulence intensity at the model height was 12.9%, and the wind speed was simulated over a range of 21.9 to 52.8 m/s (full scale). Considering the most adverse wind direction angles for the large-span flexible PV system under incoming wind and the symmetry of the structure itself, this experiment simulated wind direction angles from 0° to 30° and from 150° to 180° by rotating the turntable. The wind direction angles are arranged as shown in Fig. 2(b), with 0° representing the upper surface of the PV module facing the wind and 180° representing the lower surface facing the wind at 10° intervals. The experiment simulated three wind attack angle conditions, which were 10°, 20°, and 30°. The wind attack angle is the tilt angle of the PV module, with 10° representing a 10° angle between the PV module and the horizontal plane.

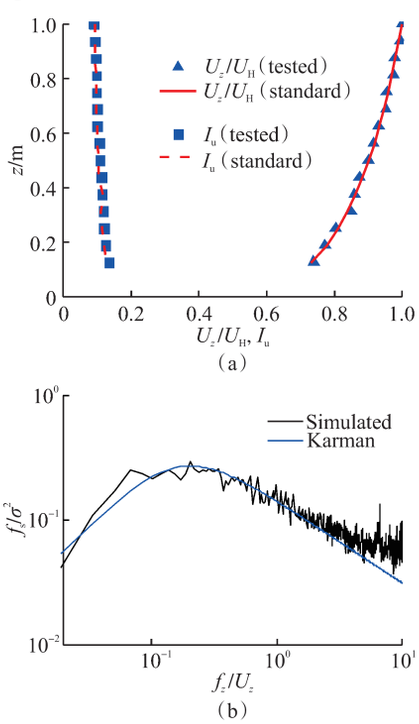

Fig. 4 Wind profile and wind spectrum simulated in a wind tunnel. (a) Wind profile; (b) Wind spectrum

2 Test Results

2.1 Vibration response and shielding effect analysis

Figs. 5 and 6 show the mean vertical displacement Z_m and the root mean square (RMS) vertical displacement values Z_{rms} of PV modules under different wind speeds for two common adverse wind direction angles when the tilt angle $\alpha = 10°$. In the downwind direction ($\theta = 0°$), the upper surface of the PV module faces the wind, causing the displacement to be downward, resulting in a negative Z_m. In the upwind direction ($\theta = 180°$), the lower surface of the PV module faces the wind, causing the displacement to be upward, resulting in a positive Z_m.

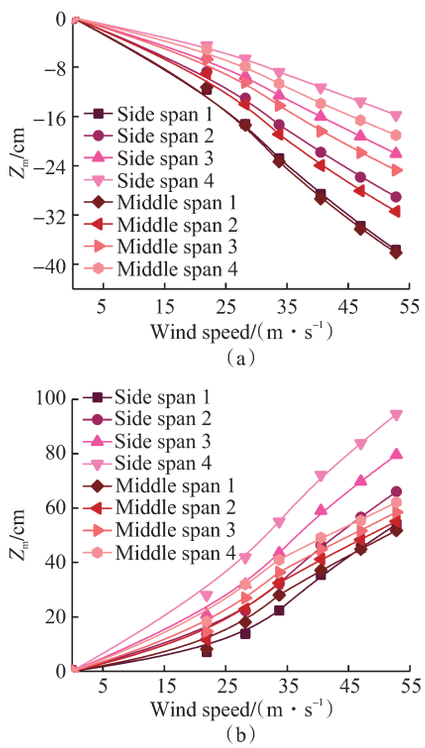

Fig. 5 Mean of vertical displacements ($\alpha = 10°$). (a) $\theta = 0°$; (b) $\theta = 180°$

From the mean displacement of the PV modules, it can be observed that the extreme values of Z_m in spans A and B occur in the windward rows. At all wind speeds, the mean displacement of the upstream PV modules is greater than that of the downstream modules, and Z_m decreases row by row, indicating that the front-row PV modules have a shielding effect on the rear rows. Conversely, the experimental results of Kim et al. [6] showed that the center rows of their cable-supported PV system may have a larger amplitude than that in the upwind rows. This discrepancy is attributed to differences in structural systems; adding horizontal linkers makes the system more integrative and the flow field around it different. As shown in Fig. 7, quantified calculations reveal that, for a wind direction angle of 0°, compared to the Z_m value of the first row, the subsequent rows de-

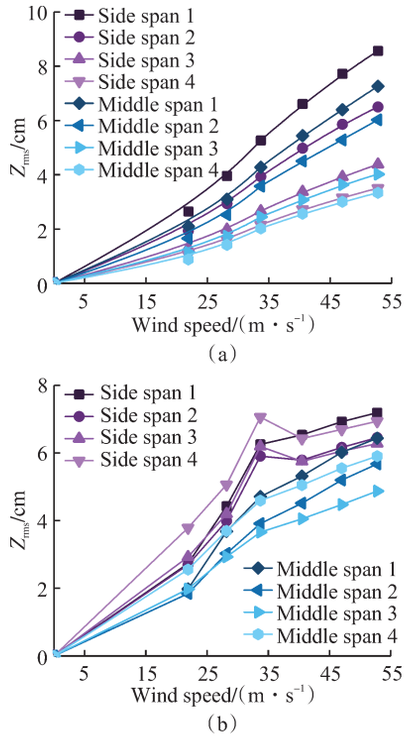

Fig. 6 RMS of vertical displacements ($\alpha = 10°$). (a) $\theta = 0°$; (b) $\theta = 180°$

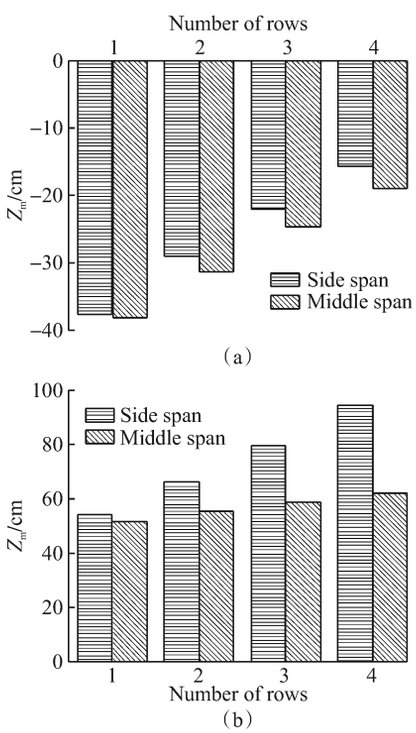

Fig. 7 Variation of the mean vertical displacement with the number of rows ($\alpha = 10°$, $U = 52.8$ m/s). (a) $\theta = 0°$; (b) $\theta = 180°$

crease by 23%, 41%, and 58% for the side span and by 18%, 35%, and 50% for the middle span. The Z_m values for the side span and middle span are similar, and the shielding effect of the front row on the rear row is also similar. For a wind direction angle of 180°, compared to

the Z_m value of the first row in the windward row, the subsequent rows decrease by 16%, 30%, and 43% for the side span and by 6%, 11%, and 17% for the middle span. The mean displacement of the first row in the windward direction of the side span is significantly greater than that of the middle span, but the shielding effect in the side span is stronger than that in the middle span, resulting in nearly identical Z_m values for the leeward rows of both spans.

From the RMS vertical displacement values of the PV modules, it can be observed that, as the wind speed increases, the vertical displacement fluctuation values of the PV modules also increase gradually, and there is no flutter phenomenon in the test wind speed range. Liu et al. [19] have experimentally evaluated the effectiveness of different types of horizontal linkers in increasing the critical wind speed for structural flutter, and the results showed that the use of horizontal linkers can significantly increase the critical wind speed compared with the nonuse of horizontal linkers. This indicates that the horizontal linkers in this study are effective in preventing the flutter instability of PV modules under strong wind conditions. Additionally, in the downwind direction, the Z_{rms} values for the side span and middle span are similar, whereas in the upwind direction, the Z_{rms} values for the side span are significantly larger than that for the middle span, which is the same as the mean vertical displacement response. Therefore, special attention should be paid to the wind-induced response of the PV modules in the side spans of multispan PV array systems in the upwind direction.

2.2 Wind-induced vibration under different wind direction angles

Existing studies have shown that the stability of flexible PV support systems is relatively poor under wind direction angles of 0° to 30°[14]. Therefore, this study also examines wind direction angles near the common adverse wind direction angles. Fig. 8 shows the mean vertical displacement of PV modules with a tilt angle of 10° and a wind speed of 52.8 m/s, as the wind direction angle varies. At different wind direction angles, the most adverse wind direction angles for spans A and B are still 0° and 180°. In the downwind direction, as the wind direction angle increases, the mean vertical displacement of the windward row in the middle span gradually becomes larger than in the side span, but it is much smaller than the mean vertical displacement in the upwind direction, and the vibration amplitude of the PV modules in the side span dominates in the upwind direction. Additionally, in the upwind direction, the mean vertical displacement in the middle span almost does not change with the wind direction angle. In other cases, the mean vertical displacement of the PV modules slightly decreases as the wind direction angle deviates from the principal wind directions (i.e., 0° and 180°).

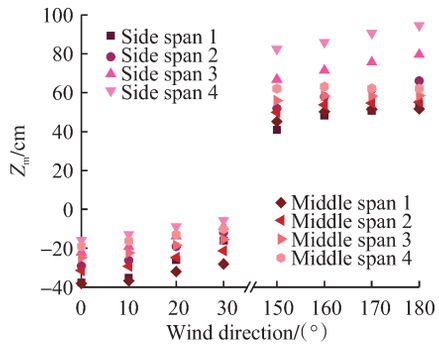

Fig. 8 Mean of vertical displacements ($\alpha = 10°$, $U = 52.8$ m/s)

Fig. 9 shows the vertical fluctuating displacement of the PV modules as the wind direction angle varies. Comparative analysis reveals that the maximum displacement fluctuation values in the first rows of the side and middle spans occur at a wind direction angle of 30°, whereas most of the other maximum displacement fluctuation values remain consistent with the wind direction angles of 0° and 180°. Considering both the mean and fluctuating displacement values, attention should be paid to multiple adverse wind direction angles, such as 0°, 30°, and 180°.

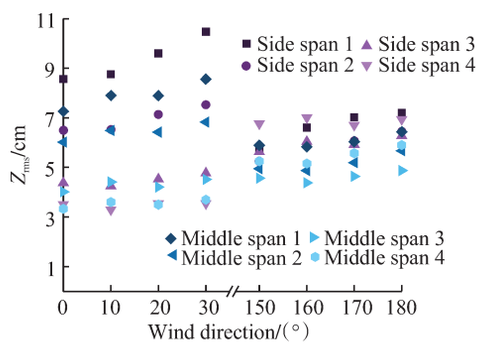

Fig. 9 RMS of vertical displacements ($\alpha = 10°$, $U = 52.8$ m/s)

2.3 Wind-induced vibration under different PV module tilt angles

Fig. 10 illustrates the mean and fluctuating vertical displacements of the windward first row under different PV module tilt angles and wind direction angles. S_{10} and M_{10} represent the side and middle spans with a PV module tilt angle of 10°, respectively. By varying the wind direction angles from 0° to 30°, it can be found that this range has little effect on the most adverse wind direction angle. Under different PV module tilt angles, the vertical displacement values of the side span are almost always greater than those of the middle span, particularly in the upwind direction. The mean displacement in the upwind direction is approximately twice that in the downwind direction; thus, the issue of wind-induced flipping of PV modules in the upwind direction needs to be considered.

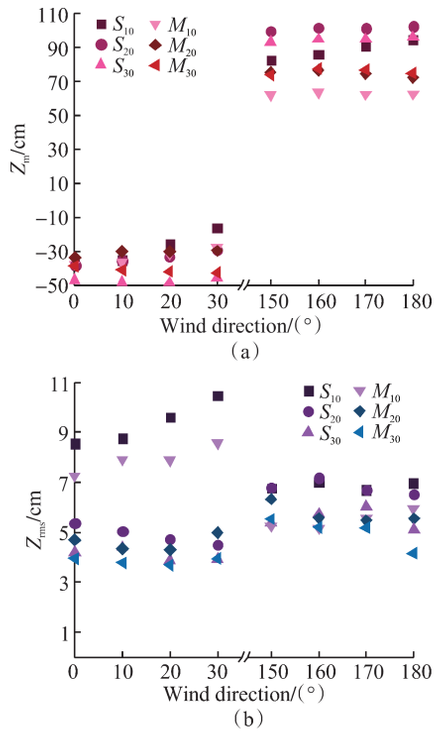

Fig. 10 Vertical displacement of the windward first row (U = 52.8 m/s). (a) Mean of vertical displacements; (b) RMS of vertical displacements

An analysis of the more significant wind-induced response of the side spans reveals that when $\theta = 0°$, the mean displacements are 1.5% and 24.8% larger at the tilt angles of 20° and 30° than that at the tilt angle of 10°, respectively. When $\theta = 180°$, the mean displacements are 8.1% and 1.6% larger at the tilt angles of 20° and 30° than that at the tilt angle of 10°, respectively. This indicates that changing the PV module tilt angle has a greater impact on the wind-induced vibration characteristics in the downwind direction and a smaller impact in the upwind direction.

3 Conclusions

(1) The flexible PV support system with double-layer cable systems can effectively control the wind-induced vibration response of the structure itself under strong wind conditions, preventing flutter. The maximum displacement of the PV array occurs in the first row facing the wind, and the upstream PV modules have a sheltering effect on the wind-induced response of the downstream PV modules, which can reach up to 23%. The wind-resistant design of the first row of such PV array structures should be strengthened.

(2) The most unfavorable wind directions for the PV array system are 0° and 180°. With the variation of wind direction angle within the range of 30°, the change in the system's wind-induced vibration response is not significant. Considering both the mean displacement and the fluctuation value, attention should be paid to the wind-induced vibration response at a wind direction angle of 30°.

(3) In the windward direction, there is little difference in the mean displacement between the side span and the middle span, whereas in the leeward direction, the displacement of the side span is much larger than that of the middle span. Special attention should be paid to the wind-resistant design of the side spans in the leeward direction.

(4) The tilt angle of the PV modules has little effect on the most unfavorable wind direction angles for the system. Changing the tilt angle of the PV modules has a greater impact on the wind-induced vibration in the windward direction and a smaller impact on that in the leeward direction.

References

[1] BAUMGARTNER F P, BÜCHEL A, BARTHOLET R. Solar wings: A new lightweight PV tracking system[C]// 23rd European Photovoltaic Solar Energy Conference. Winterthur, Switzerland, 2008: 2790-2794.

[2] TAO T Y, GAO W J, JIANG Z X, et al. Analysis on wind-induced vibration and its influential factors of long suspenders in the wake of bridge tower[J]. Journal of Southeast University (Natural Science Edition), 2023, 53(6): 1065-1071. (in Chinese)

[3] LANG T Y, WANG H, JIA H Z, et al. Vortex-induced vibration performance and wind pressure distribution of main girder of long-span suspension bridge affected by temporary facilities[J]. Journal of Southeast University (Natural Science Edition), 2022, 52(5): 833-840. (in Chinese)

[4] WANG H, YANG M, TAO T Y, et al. Parameter sensitivity analysis on dynamic characteristics of long-span quadruple-tower suspension bridge[J]. Journal of Southeast University (Natural Science Edition), 2016, 46(3): 559-564. (in Chinese)

[5] TAMURA Y, KIM Y C, YOSHIDA A, et al. Wind-induced vibration experiment on solar wing[C]// MATEC Web of Conferences. Prague, Czech, 2015, 24: 04006.

[6] KIM Y C, TAMURA Y, YOSHIDA A, et al. Experimental investigation of aerodynamic vibrations of solar wing system[J]. Advances in Structural Engineering, 2018, 21(15): 2217-2226.

[7] WANG Z G, ZHAO F F, JI C M, et al. Analysis of vibration control of multi-row large-span flexible photovoltaic supports[J]. Engineering Journal of Wuhan University, 2020, 53(S1): 29-34. (in Chinese)

[8] WANG Z G, ZHAO F F, JI C M, et al. Wind-induced vibration analysis of multi-row and multi-span flexible photovoltaic support[J]. Engineering Journal of Wuhan University, 2021, 54(S2): 75-79. (in Chinese)

[9] LIU Z C. Mechanical behavior of flexible photovoltaic support with elastic wind resistant cable[D]. Nanjing: Southeast University, 2021. (in Chinese)

[10] CHAI X B. Research on wind loads on flexible solar photovoltaic support system [D]. Shijiazhuang: Shijia-

zhuang Tiedao University, 2020.(in Chinese)
[11] MA W Y, CHAI X B, MA C C, et al. Experimental study of wind load influencing factors of flexible support photovoltaic modules[J]. Acta Energiae Solaris Sinica, 2021, 42(11): 10-18.(in Chinese)
[12] WANG X M. Study on the influence factors of wind load of photovoltaic arrays[D]. Changsha: Central South University, 2022.(in Chinese)
[13] YANG Y M. Study on wind-induced vibration of large-span flexible support structures in photovoltaic power plants[D]. Kunming: Kunming University of Science and Technology, 2023.(in Chinese)
[14] CHEN Q, NIU H W, LI H X, et al. Aerodynamic stability and interference effect on a flexible photovoltaic based on wind tunnel test with aeroelastic model[J]. Journal of Building Structures, 2023, 44(11): 153-161.(in Chinese)
[15] XU H W, LI J L, HE X H, et al. Aero-elastic experiment investigation on the aerodynamic damping of large-span single-layer cable-suspended photovoltaic modules[J]. Journal of Vibration and Shock, 2024, 43(10): 21-29.(in Chinese)
[16] ZHOU R, WANG H, XU Z D, et al. Wind-resistance reliability assessment of flexible photovoltaic support in region prone to strong wind[J]. Journal of Southeast University (Natural Science Edition), 2024, 54(4): 845-851.(in Chinese)
[17] HE X H, DING H, JING H Q, et al. Wind-induced vibration and its suppression of photovoltaic modules supported by suspension cables[J]. Journal of Wind Engineering and Industrial Aerodynamics, 2020, 206: 104275.
[18] DING H, HE X H, JING H Q, et al. Design method of primary structures of a cost-effective cable-supported photovoltaic system[J]. Applied Sciences, 2023, 13(5): 2968.
[19] LIU J Q, LI S Y, LUO J, et al. Experimental study on critical wind velocity of a 33-meter-span flexible photovoltaic support structure and its mitigation[J]. Journal of Wind Engineering and Industrial Aerodynamics, 2023, 236: 105355.
[20] LI J L, HONG G H, XU H W. Wind load effects and gust loading factor for cable-suspended photovoltaic structures[J]. Energies, 2023, 17(1): 38.
[21] WANG W, CAO J X, CAO S Y. Wind vibration characteristics of array-type flexible photovoltaic system[J/OL]. Engineering Mechanics, 2024[2024-09-01]. http://engineeringmechanics.cn/cn/article/doi/10.6052/j.issn.1000-4750.2023.11.0873.(in Chinese)
[22] FU X, REN R X, LI J, et al. Experimental and numerical study on the aerodynamic characteristics of a double-row photovoltaic panel[J]. Journal of Wind Engineering and Industrial Aerodynamics, 2024, 253: 105846.

多跨间双层索系光伏支架结构风振响应特性分析

邹良浩[1], 王健[1], 宋杰[1], 周锐[2], 王浩[2]

(1.武汉大学土木建筑工程学院, 武汉 430072; 2.东南大学混凝土及预应力混凝土结构教育部重点实验室, 南京 211189)

摘要: 为探究多跨间双层索系光伏支架结构的风致振动响应特性,采用气动弹性模型风洞试验,得到三跨四排双层索系柔性光伏支架系统的风致响应数据,并分析了不同光伏组件倾角、风速和风向角下的风致振动特性。结果表明,双层索系大跨度柔性光伏支架在强风下能有效控制风致振动响应,预防颤振现象的发生。柔性光伏支架系统的风致振动位移最大值出现在迎风首排。上游组件对下游组件存在显著的遮挡效果,其效果最大可达23%。结构最不利风向角为0°和180°,在0°~30°范围内风向角的变化对风振响应影响不大。光伏组件倾角的变化对顺风向风致振动影响较大,对逆风向影响较小。结构设计时,应特别关注逆风向侧跨的结构抗风设计。

关键词: 双层索系;光伏支架;气动弹性模型;风洞试验;风振响应

中图分类号: TU399